

Dynamics of Frenkel excitons in pentacene

Sonja Gombar, Petar Mali, Milan Pantić, Milica Pavkov-Hrvojević, and Slobodan Radošević
Department of Physics, Faculty of Sciences, University of Novi Sad, Trg Dositeja Obradovića 4, Novi Sad, Serbia

The dispersion relation for noninteracting excitons and the influence of perturbative correction is examined in the case of pentacene structure. The values of exchange integrals are determined by the nonlinear fits to the experimental dispersion data obtained by inelastic electron scattering in Phys. Rev. Lett. **98**, 037402 (2007). We obtain theoretical dispersion curves along four different directions in the Brillouin zone which possess the same periodicity as the experimental data. We also showed that perturbative corrections are negligible since the exciton gap in dispersion relation is huge in comparison to exchange integrals.

I. INTRODUCTION

In the last few decades organic molecular solids have been matter of intense theoretical and experimental studies, due to their potential applications in novel organic devices [1, 2]. The recent advances in experimental methods have provided detailed insight into their microscopic properties [3]. Among the energetically lowest excitations in such systems are Frenkel excitons, electron-hole pairs of small radius [4]. The general theory of Frenkel excitons in molecular crystals is exposed in detail in [5], while some references on applications and progress are [6–9].

The method of inelastic electron scattering was used for direct measurement of the exciton band structure within the reciprocal $\mathbf{a}^*\mathbf{b}^*$ plane of pentacene at room temperature ($T = 300\text{K}$) in [3]. Results of measurements along four different directions in the Brillouin zone were presented and, on that basis, the authors of [3] argued that the model of noninteracting Frenkel excitons is inapplicable for description of pentacene (see also [10] for measurements at $T = 20\text{K}$ and [11] for similar experiments on picene). They also suggested that the charge-transfer (CT) excitons must be included in model Hamiltonian of pentacene in order to achieve better agreement with experiment. Following these experiments, a significant theoretical work was conducted in order to obtain properties of pentacene from the first principles, i.e. starting from many-body electron-hole Hamiltonians [12–16].

The present paper deals with the problem of obtaining exciton dispersion in pentacene by relying on a correspondence between Paulion Hamiltonian and anisotropic XXZ Heisenberg ferromagnet. Unlike previous theoretical works, based on many-body Hamiltonians containing electron and hole creation and annihilation operators, we present calculations based on effective Hamiltonian [17–19]. In other words, we start from Frenkel excitons as low lying degrees of freedom and obtain effective form of their interactions which are considered to the one loop order.

Whereas our results confirm that exciton dispersion in pentacene can not be described within Frenkel model alone in satisfactory manner, they also suggest that the influence of other excitations may not be as large as originally proposed.

The paper is organized as follows. The model Hamiltonian and pentacene structure are introduced in Sec.

II, while exciton dispersion in noninteracting model is obtained in Sec. III. Finally, we discuss the effects of exciton-exciton interactions within two-level model in Sec. IV and V.

II. MODEL HAMILTONIAN AND PENTACENE STRUCTURE

The basic Hamiltonian that governs the dynamics of excitons in two-level system (only one electronically excited molecular state is considered) is given by

$$H = H_0 + \Delta \sum_{\mathbf{n}} P_{\mathbf{n}}^+ P_{\mathbf{n}} - \frac{X}{2} \sum_{\mathbf{n}, \boldsymbol{\lambda}} P_{\mathbf{n}}^+ P_{\mathbf{n}+\boldsymbol{\lambda}} - \frac{Y}{2} \sum_{\mathbf{n}, \boldsymbol{\lambda}} P_{\mathbf{n}}^+ P_{\mathbf{n}} P_{\mathbf{n}+\boldsymbol{\lambda}}^+ P_{\mathbf{n}+\boldsymbol{\lambda}}. \quad (1)$$

where $P_{\mathbf{n}}^+$ and $P_{\mathbf{n}}$ are standard Pauli operators on the site \mathbf{n} and X and Y are parameters describing hopping and interactions of excitons, respectively [5, 20]. Using the exact one to one correspondence between Pauli and spin operators in the case of $S = 1/2$ [21], we obtain anisotropic (XXZ) Heisenberg Hamiltonian in external field

$$H = -\frac{I^x}{2} \sum_{\mathbf{n}, \boldsymbol{\lambda}} S_{\mathbf{n}}^- S_{\mathbf{n}+\boldsymbol{\lambda}}^+ - \frac{I^z}{2} \sum_{\mathbf{n}, \boldsymbol{\lambda}} S_{\mathbf{n}}^z S_{\mathbf{n}+\boldsymbol{\lambda}}^z - \mu \mathcal{H} \sum_{\mathbf{n}} S_{\mathbf{n}}^z, \quad (2)$$

where $\{\boldsymbol{\lambda}\}$ denotes vectors connecting neighboring sites, z_1 is the number of nearest neighbours and

$$I^z = Y, \quad I^x = X, \quad \mu \mathcal{H} = \Delta - \frac{I^z z_1}{2}. \quad (3)$$

Equivalently, inverse relations are

$$\Delta = \frac{I^z z_1}{2} + \mu \mathcal{H}, \quad Y = I^z, \quad X = I^x, \\ H_0 = -\frac{I^z N z_1}{8} - \frac{N \mu \mathcal{H}}{2}. \quad (4)$$

Due to the isomorphism of spin and paulion Hilbert spaces on every lattice site and relations (3)-(4), the original problem of exciton dynamics governed by (1) can be completely mapped on the equivalent effective spin model (2). It should be noted that this correspondence is purely formal – it will allow us to investigate the exciton system with the help of a vast number of existing theoretical tools developed for spin systems [21–29]. According to [5], Pauli Hamiltonian (1), which is as we have

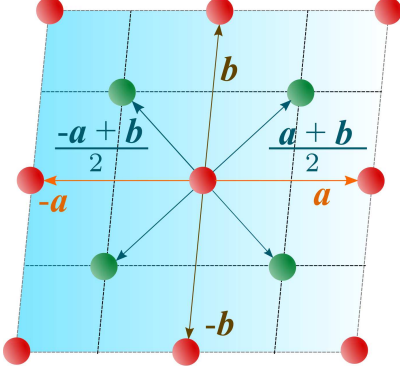


FIG. 1. Schematic presentation of the pentacene lattice. A pair of exchange integrals corresponds to the each set of lattice vectors $\{\mathbf{a}, -\mathbf{a}\}$, $\{\mathbf{b}, -\mathbf{b}\}$ and $\{\frac{\mathbf{a}+\mathbf{b}}{2}, -\frac{\mathbf{a}+\mathbf{b}}{2}, -\frac{\mathbf{a}-\mathbf{b}}{2}, -\frac{\mathbf{a}-\mathbf{b}}{2}\}$ (see text).

shown here equivalent to anisotropic Heisenberg Hamiltonian (2), can be used in description of pentacene. This fact will enable us to examine dispersion of noninteracting excitons as well as the influence of their interactions in leading order (one-loop) approximation. One should also note that, in many practical cases, the set of neighboring sites connected with hopping integrals splits into several subsets, determined by the lattice structure and values of hopping parameters.

We shall analyze now the pentacene structure. A schematic sketch of the pentacene thin film lattice is shown in Figure 1. The lattice parameters within the \mathbf{ab} layer of the single crystal of pentacene are $|\mathbf{a}| = 6.27\text{\AA}$, $|\mathbf{b}| = 7.78\text{\AA}$, $\angle(\mathbf{a}, \mathbf{b}) = 87.8^\circ$ [30]. Central motive in Figure 1 has three types of neighbours: two neighbours at points $\lambda_1 = \{\mathbf{a}, -\mathbf{a}\}$ coupled through exchange integral I_1 , two neighbours at points $\lambda_2 = \{\mathbf{b}, -\mathbf{b}\}$ coupled through exchange integral I_2 and four neighbours at points $\lambda_3 = \{\frac{\mathbf{a}+\mathbf{b}}{2}, -\frac{\mathbf{a}+\mathbf{b}}{2}, -\frac{\mathbf{a}-\mathbf{b}}{2}, -\frac{\mathbf{a}-\mathbf{b}}{2}\}$ coupled via exchange integral I_3 . As we have already noted, the transition from Pauli to Heisenberg Hamiltonian requires anisotropic exchange integrals. Therefore, each of the mentioned exchange integrals splits into x and z components: $I_j \rightarrow (I_j^x, I_j^z)$, where $j = 1, 2$ or 3 . The results from a recent paper [31] show that the most important hopping paths in the pentacene crystal are in the planes perpendicular to the \mathbf{c}^* axis. Thus, to a good approximation, real pentacene crystal can be effectively described by a two dimensional model. Finally, by following common practice [3], we shall present numerical results for the approximate pentacene lattice, defined by the additional constraint $\mathbf{a} \cdot \mathbf{b} = 0$.

III. DISPERSION OF NONINTERACTING EXCITONS

Bearing in mind remarks on pentacene structure from previous section, we obtain Hamiltonian (2), adapted to

the pentacene structure, in the Bloch approximation,

$$\begin{aligned}
 H &= H'_0 - \frac{1}{2} \sum_j I_j^x \sum_{\mathbf{n}, \lambda_j} B_{\mathbf{n}}^\dagger B_{\mathbf{n}+\lambda_j} + \frac{1}{2} \sum_j I_j^z \sum_{\mathbf{n}, \lambda_j} B_{\mathbf{n}}^\dagger B_{\mathbf{n}} \\
 &+ \mu \mathcal{H} \sum_{\mathbf{n}} B_{\mathbf{n}}^\dagger B_{\mathbf{n}} \\
 &= H'_0 - \frac{I_1^x}{2} \sum_{\mathbf{n}, \lambda_1} B_{\mathbf{n}}^\dagger B_{\mathbf{n}+\lambda_1} + \frac{I_1^z}{2} \sum_{\mathbf{n}, \lambda_1} B_{\mathbf{n}}^\dagger B_{\mathbf{n}} \\
 &- \frac{I_2^x}{2} \sum_{\mathbf{n}, \lambda_2} B_{\mathbf{n}}^\dagger B_{\mathbf{n}+\lambda_2} + \frac{I_2^z}{2} \sum_{\mathbf{n}, \lambda_2} B_{\mathbf{n}}^\dagger B_{\mathbf{n}} \\
 &- \frac{I_3^x}{2} \sum_{\mathbf{n}, \lambda_3} B_{\mathbf{n}}^\dagger B_{\mathbf{n}+\lambda_3} + \frac{I_3^z}{2} \sum_{\mathbf{n}, \lambda_3} B_{\mathbf{n}}^\dagger B_{\mathbf{n}} \\
 &+ \mu \mathcal{H} \sum_{\mathbf{n}} B_{\mathbf{n}}^\dagger B_{\mathbf{n}}, \tag{5}
 \end{aligned}$$

where $B_{\mathbf{n}}^\dagger$ ($B_{\mathbf{n}}$) are boson creation (annihilation) operators. The same Hamiltonian in \mathbf{k} space has the form:

$$\begin{aligned}
 \tilde{H} &= \tilde{H}'_0 - \frac{I_1^x}{2} \sum_{\mathbf{k}} B_{\mathbf{k}}^\dagger B_{\mathbf{k}} z_1 \gamma_1(\mathbf{k}) + \frac{I_1^z z_1}{2} \sum_{\mathbf{k}} B_{\mathbf{k}}^\dagger B_{\mathbf{k}} \\
 &- \frac{I_2^x}{2} \sum_{\mathbf{k}} B_{\mathbf{k}}^\dagger B_{\mathbf{k}} z_2 \gamma_2(\mathbf{k}) + \frac{I_2^z z_2}{2} \sum_{\mathbf{k}} B_{\mathbf{k}}^\dagger B_{\mathbf{k}} \\
 &- \frac{I_3^x}{2} \sum_{\mathbf{k}} B_{\mathbf{k}}^\dagger B_{\mathbf{k}} z_3 \gamma_3(\mathbf{k}) + \frac{I_3^z z_3}{2} \sum_{\mathbf{k}} B_{\mathbf{k}}^\dagger B_{\mathbf{k}} \\
 &+ \mu \mathcal{H} \sum_{\mathbf{k}} B_{\mathbf{k}}^\dagger B_{\mathbf{k}}, \tag{6}
 \end{aligned}$$

where $z_1 = z_2 = 2$, $z_3 = 4$ and corresponding geometric factors are defined by

$$\begin{aligned}
 \gamma_1(\mathbf{k}) &= \frac{1}{2} \sum_{\lambda_1} e^{i\mathbf{k} \cdot \lambda_1} = \frac{1}{2} (e^{i\mathbf{k} \cdot \mathbf{a}} + e^{-i\mathbf{k} \cdot \mathbf{a}}) = \cos(\mathbf{k} \cdot \mathbf{a}), \tag{7} \\
 \gamma_2(\mathbf{k}) &= \frac{1}{2} \sum_{\lambda_2} e^{i\mathbf{k} \cdot \lambda_2} = \frac{1}{2} (e^{i\mathbf{k} \cdot \mathbf{b}} + e^{-i\mathbf{k} \cdot \mathbf{b}}) = \cos(\mathbf{k} \cdot \mathbf{b}), \tag{8} \\
 \gamma_3(\mathbf{k}) &= \frac{1}{4} \sum_{\lambda_3} e^{i\mathbf{k} \cdot \lambda_3} \\
 &= \frac{1}{4} (e^{i\mathbf{k} \cdot \frac{\mathbf{a}+\mathbf{b}}{2}} + e^{-i\mathbf{k} \cdot \frac{\mathbf{a}+\mathbf{b}}{2}} + e^{i\mathbf{k} \cdot \frac{\mathbf{a}-\mathbf{b}}{2}} + e^{-i\mathbf{k} \cdot \frac{\mathbf{a}-\mathbf{b}}{2}}) \\
 &= \frac{1}{2} \cos \left[\frac{\mathbf{k} \cdot (\mathbf{a} + \mathbf{b})}{2} \right] + \frac{1}{2} \cos \left[\frac{\mathbf{k} \cdot (\mathbf{a} - \mathbf{b})}{2} \right] \\
 &= \cos \left(\frac{\mathbf{k} \cdot \mathbf{a}}{2} \right) \cos \left(\frac{\mathbf{k} \cdot \mathbf{b}}{2} \right). \tag{9}
 \end{aligned}$$

From

$$\tilde{H} = \tilde{H}'_0 + \sum_{\mathbf{k}} E(\mathbf{k}) B_{\mathbf{k}}^\dagger B_{\mathbf{k}} \tag{10}$$

we obtain dispersion relation

$$\begin{aligned}
 E(\mathbf{k}) &= I_1^x \left[\frac{I_1^z}{I_1^x} - \cos(\mathbf{k} \cdot \mathbf{a}) \right] + I_2^x \left[\frac{I_2^z}{I_2^x} - \cos(\mathbf{k} \cdot \mathbf{b}) \right] \\
 &+ 2I_3^x \left[\frac{I_3^z}{I_3^x} - \cos \left(\frac{\mathbf{k} \cdot \mathbf{a}}{2} \right) \cos \left(\frac{\mathbf{k} \cdot \mathbf{b}}{2} \right) \right] + \mu \mathcal{H}.
 \end{aligned}$$

That is,

$$E(\mathbf{k}) = \Delta - I_1^x \cos(\mathbf{k} \cdot \mathbf{a}) - I_2^x \cos(\mathbf{k} \cdot \mathbf{b}) - 2I_3^x \cos\left(\frac{\mathbf{k} \cdot \mathbf{a}}{2}\right) \cos\left(\frac{\mathbf{k} \cdot \mathbf{b}}{2}\right), \quad (11)$$

where we have defined the exciton gap

$$\Delta = I_1^z + I_2^z + 2I_3^z + \mu\mathcal{H}. \quad (12)$$

Exciton dispersion (11) law is plotted along (100) in Fig. 2. Note that the orthogonality condition $\mathbf{a} \cdot \mathbf{b} = 0$ allows us to determine $I_1^x = 5.7\text{meV}$ and $I_3^x = 23.4\text{meV}$ by fitting (11) to experimental data along this direction only (see the paper [32] for a discussion on determination of exchange integrals from dispersion relation in a similar context). The value $\Delta = 1.83\text{eV}$ is taken from [33]. The last parameter $I_2^x = 3.4\text{meV}$ is extracted from the experimental data on exciton dispersion along (210) direction (see Fig. 3). By using this set of parameters, we have plotted the exciton dispersion along (110) and (120) directions and compared them to the experimental data from [3]. Since we have used a single set of model parameters, the plotted dispersion law displays the unique limit $\Delta - I_1^x - I_2^x - 2I_3^x = 1.7741\text{eV}$ as $|\mathbf{k}| \rightarrow 0$ for all four directions in Brillouin zone. This is clearly seen from Figs 2, 3, 4 and 5. Finally, 3D plot of exciton dispersion $E(k_x, k_y)$ is given in Fig. 6.

The disagreement between dispersion of excitons predicted by the noninteracting Frenkel model and experimental data, which is evident from Figs 2, 3, 4 and 5, should be attributed to the existence of other excitations (CT excitons) in the system according to [3]. Specifically, the difference between theoretical curve and experiment was the most prominent along (120) direction in [3], since calculated and measured dispersion do not share the same periodicity. Even though the agreement between theory and experiment is the best for (100) direction, theoretical curves presented here possess the same periodicity as experimental data within Brillouin zone, for all four directions. Thus, the influence of CT excitons may not be as large as originally suggested in [3].

The exciton dispersion in paper [3] is given by

$$E(\mathbf{k}) = E_0 + t_a \cos(\mathbf{k} \cdot \mathbf{a}) + t_b \cos(\mathbf{k} \cdot \mathbf{b}) + 2t_{ab} \cos\left(\frac{\mathbf{k} \cdot \mathbf{a}}{2}\right) \cos\left(\frac{\mathbf{k} \cdot \mathbf{b}}{2}\right). \quad (13)$$

Since the effective mass of excitons in pentacene is large [34], hopping parameters in (1) are positive and small so that corresponding Heisenberg Hamiltonian (2) describes a ferromagnet. By comparing relations (11) and (13) we find

$$t_a = -I_1^x < 0, \quad t_b = -I_2^x < 0, \quad t_{ab} = -I_3^x < 0. \quad (14)$$

Therefore, without fitting dispersion on experimental data, we conclude that t_a , t_b , t_{ab} must be negative, which is in accordance with [3].

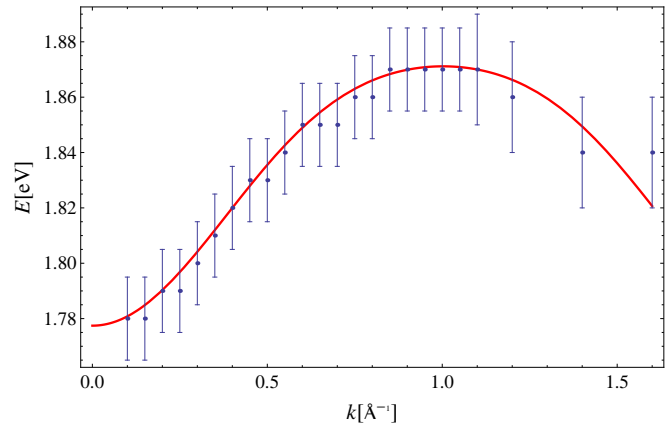


FIG. 2. Exciton dispersion along (100) direction. Experimental data are taken from [3]. Theoretical curve is obtained for: $\Delta = 1.83\text{eV}$ [33], $I_1^x = 5.7\text{meV}$ and $I_3^x = 23.4\text{meV}$.

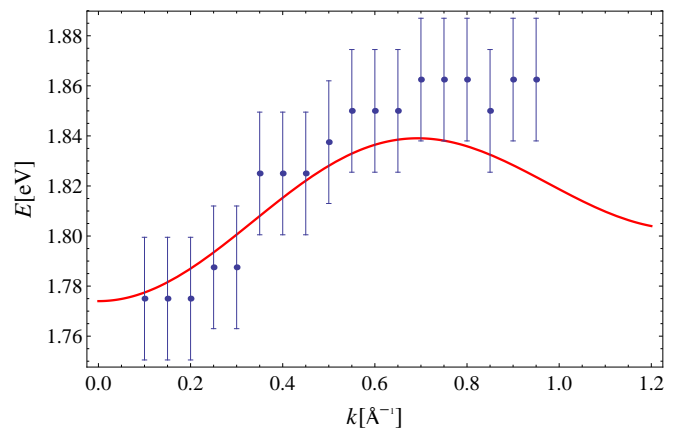


FIG. 3. Exciton dispersion along (210) direction. Experimental data are taken from [3]. Theoretical curve is obtained for: $I_2^x = 3.4\text{meV}$ (the rest of the parameters are as in Fig. 2).

IV. PERTURBATIVE CORRECTIONS

In the previous section we saw that the model of noninteracting excitons gives dispersion law which lies within error bars almost within entire Brillouin zone. The question, which naturally follows this observation, is: could the agreement between theory and experiment be improved by including the effects of exciton-exciton interactions? By answering to this question we could provide additional support for the hypothesis proposed for the first time in [3], according to which additional excitations (CT excitons) need to be taken into account for correct description of pentacene.

A careful examination of traditional methods for studying the effect of interactions in models based on Pauli/Heisenberg Hamiltonians (1) - (2) reveals that they possess certain flaws. To avoid them, we employ perturbation theory developed in [35, 36]. The main advantage of this method is that boson representations of spin operators are unnecessary. In other words, exciton-exciton interaction, which is partially hidden in the spin Hamiltonian and partially in the corresponding Hilbert space, is explicitly given through interaction pieces of

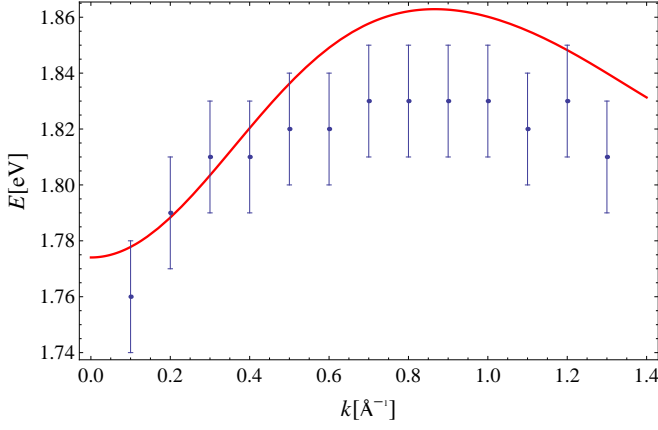


FIG. 4. Exciton dispersion along (120) direction. Experimental data are taken from [3]. Parameters used for theoretical fit are as in Figures 2 and 3.

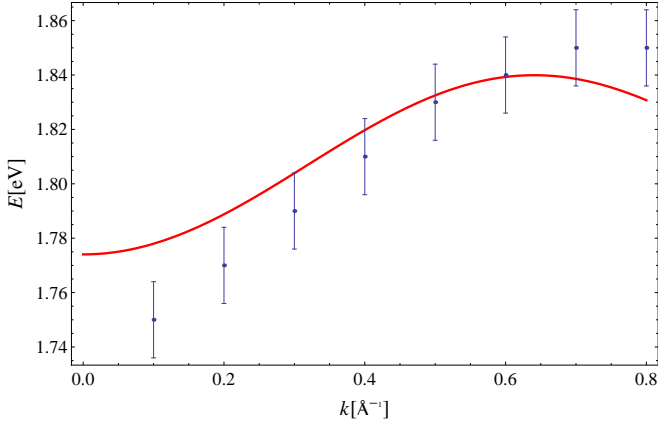


FIG. 5. Exciton dispersion along (110) direction. Experimental data are taken from [3]. Parameters used for theoretical fit are as in Figures 2 and 3.

Lagrangian. Therefore, perturbative corrections may be calculated more systematically. This is extremely important for $S = 1/2$ spin Hamiltonians, since $1/S$ is not a small parameter that can control perturbative calculations.

As it is well known, the Lagrangian that reproduces

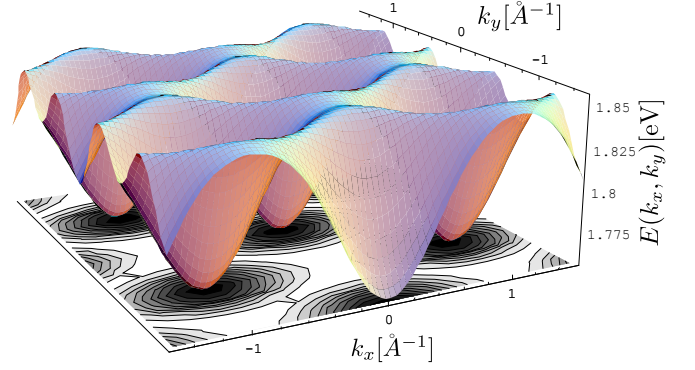


FIG. 6. Exciton dispersion in three dimensions. Parameters used for theoretical fit are as in Figures 2 and 3.

Landau-Lifshitz equation is [18, 37, 38]

$$\mathcal{L}_{\text{eff}} = \Sigma \frac{\partial_t U^1 U^2 - \partial_t U^2 U^1}{1 + U^3} - \frac{F^2}{2} \partial_\alpha U^i \partial_\alpha U^i + \Sigma \mu \mathcal{H} U^3 \quad (15)$$

where two excitation fields are collected into the unit vector $\mathbf{U} := [U^1 \ U^2 \ U^3]^T \equiv [\boldsymbol{\pi}(x), U^3(x)]^T$, $\Sigma = NS/V$ and F is a constant to be determined later.

Corresponding free part of Lagrangian is

$$\mathcal{L}_{\text{free}} = \frac{\Sigma}{2} [\partial_t \pi^1 \pi^2 - \partial_t \pi^2 \pi^1] + \frac{F^2}{2} \boldsymbol{\pi} \cdot \partial_\alpha \partial_\alpha \boldsymbol{\pi} + \Sigma \mu \mathcal{H} \pi^2 \quad (16)$$

and interaction part up to quartic approximation (which is sufficient for one loop calculations) is

$$\mathcal{L}_{\text{int}} = \frac{F^2}{8} \boldsymbol{\pi}^2 \partial_\alpha \partial_\alpha \boldsymbol{\pi}^2 - \frac{F^2}{8} \boldsymbol{\pi}^2 \boldsymbol{\pi} \cdot \partial_\alpha \partial_\alpha \boldsymbol{\pi}. \quad (17)$$

To obtain the Hamiltonian suitable for perturbative calculation, we apply canonical quantization and incorporate the structure of the lattice presented at Fig. 1. Basically this means that we wish to construct the free Hamiltonian with lattice exciton fields that reproduces exciton dispersion (11)

$$H_0 = -\frac{v_0}{2m} \sum_{\mathbf{x}} \psi^\dagger D^2 \psi + \mu \mathcal{H} v_0 \sum_{\mathbf{x}} \psi^\dagger \psi, \quad (18)$$

where $v_0 = ab$, ψ and ψ^\dagger satisfy canonical commutation relations for Schrodinger fields and D^2 and m are the discrete Laplacian and parameter defined in such a way for (18) to reproduce dispersion (11). It can be readily checked that D^2 is given by

$$D^2 = \nabla_{(3)}^2 + \frac{1}{2} \frac{|\boldsymbol{\lambda}_1|^2}{|\boldsymbol{\lambda}_3|^2} \frac{I_1^x}{I_3^x} \nabla_{(1)}^2 + \frac{1}{2} \frac{|\boldsymbol{\lambda}_2|^2}{|\boldsymbol{\lambda}_3|^2} \frac{I_2^x}{I_3^x} \nabla_{(2)}^2, \quad (19)$$

where

$$\nabla_{(j)}^2 \phi(\mathbf{x}) := \frac{4}{z_j |\boldsymbol{\lambda}_j|^2} \sum_{\boldsymbol{\lambda}_j} \left(\phi(\mathbf{x} + \boldsymbol{\lambda}_j) - \phi(\mathbf{x}) \right), \quad (20)$$

$$j = 1, 2, 3$$

are the discrete Laplacians for three sets of neighbors (see the Fig. 1) and

$$m = \frac{1}{I_3^x |\boldsymbol{\lambda}_3|^2} \equiv \frac{\Sigma}{2F^2}. \quad (21)$$

Further, it is useful to introduce eigenvalues of discrete Laplacians. They are given by

$$\nabla_{(j)}^2 e^{i\mathbf{k} \cdot \mathbf{x}} = -\widehat{\mathbf{k}}_{(j)}^2 e^{i\mathbf{k} \cdot \mathbf{x}}, \quad (22)$$

$$\widehat{\mathbf{k}}_{(j)}^2 := \frac{2D}{|\boldsymbol{\lambda}_j|^2} \left(1 - \gamma_j(\mathbf{k}) \right)$$

$$E(\mathbf{k}) = \mu\mathcal{H} + \delta_1 + \delta_2 + \delta_3 + \frac{I_3^x |\lambda_3|^2}{2} \left[\widehat{\mathbf{k}}_{(3)}^2 + \frac{1}{2} \frac{|\lambda_1|^2}{|\lambda_3|^2} \frac{I_1^x}{I_3^x} \widehat{\mathbf{k}}_{(1)}^2 + \frac{1}{2} \frac{|\lambda_2|^2}{|\lambda_3|^2} \frac{I_2^x}{I_3^x} \widehat{\mathbf{k}}_{(2)}^2 \right] \equiv \Delta + \frac{\widehat{\mathbf{k}}^2}{2m} \quad (23)$$

where $\delta_j = I_j^z - I_j^x$. Thus, Hamiltonian (18) is equivalent to the Bloch Hamiltonian (10). Note that the discrete Laplacian D^2 , which defines local changes of the excitation fields, depends on ratios I_1^x/I_3^x and I_2^x/I_3^x . Thus, the full symmetry of the pentacene lattice, which reflects itself through the energies of free excitons, can be implemented within effective model only by the right choice of exchange integrals. The exciton-exciton interactions, which modify exciton dispersion to the one loop can now be written as (see [35, 36])

$$H_{\text{int}} = H_4^{(a)} + H_4^{(b)}, \quad (24)$$

with

$$H_4^{(a)} = \frac{F^2}{8} v_0 \sum_{\mathbf{x}} \pi^2(\mathbf{x}) \boldsymbol{\pi}(\mathbf{x}) \cdot D^2 \boldsymbol{\pi}(\mathbf{x}), \quad (25)$$

$$H_4^{(b)} = -\frac{F^2}{8} v_0 \sum_{\mathbf{x}} \pi^2(\mathbf{x}) D^2 \pi^2(\mathbf{x}),$$

and

$$\psi = \sqrt{\frac{2}{\Sigma}} \left[\pi^2 + i\pi^2 \right]. \quad (26)$$

Now we can calculate the one-loop correction to the exciton dispersion. It is determined by the one-loop self energy which, in turn, may be calculated by the diagrammatic rules introduced in [35, 36]. In short, we see from (25) that the excitons are coupled derivatively so that internal and external lines on Feynman diagrams carry eigenvalues of discrete Laplacians [17]. These are denoted by colored propagator lines. The exciton propagator, written in Matsubara formalism, is given by

$$\begin{aligned} D(\mathbf{x} - \mathbf{y}, \tau_x - \tau_y) &= \langle T \{ \psi(\mathbf{x}, \tau_x) \psi^\dagger(\mathbf{y}, \tau_y) \} \rangle_0 \quad (27) \\ &= \frac{1}{\beta} \sum_{n=-\infty}^{\infty} \int_{\mathbf{q}} \frac{e^{i\mathbf{q} \cdot (\mathbf{x} - \mathbf{y}) - i\omega_n (\tau_x - \tau_y)}}{E(\mathbf{q}) - i\omega_n}, \end{aligned}$$

where

$$\int_{\mathbf{q}} \equiv \int_{\text{IBZ}} \frac{d^D \mathbf{q}}{(2\pi)^D}. \quad (28)$$

Within one-loop approximation, there are four types of diagrams. They can be easily evaluated

$$\begin{aligned} \text{Diagram 1} &= \text{Diagram 2} + \text{Diagram 3} = \frac{1}{S} \frac{v_0}{2m_0} \int_{\mathbf{p}} \langle n_{\mathbf{q}} \rangle_0 \left[\widehat{\mathbf{k}}^2 + \widehat{\mathbf{p}}^2 \right], \quad (29) \end{aligned}$$

$$\begin{aligned} \text{Diagram 4} &= \text{Diagram 5} + \text{Diagram 6} = -\frac{1}{S} \frac{v_0}{2m_0} \int_{\mathbf{p}} \langle n_{\mathbf{p}} \rangle_0 \widehat{\mathbf{k} - \mathbf{p}}^2, \quad (30) \end{aligned}$$

with $\widehat{\mathbf{k}}^2$ defined in (23) and $\langle n_{\mathbf{p}} \rangle_0$ denoting the free exciton Bose distribution. Explicit expression for exciton self-energy is found by using relation

$$\int_{\mathbf{q}} \langle n_{\mathbf{q}} \rangle_0 \widehat{\mathbf{p} - \mathbf{q}}_{(j)}^2 = \int_{\mathbf{q}} \langle n_{\mathbf{q}} \rangle_0 \left[\widehat{\mathbf{p}}_{(j)}^2 + \widehat{\mathbf{q}}_{(j)}^2 - \frac{|\lambda_j|^2}{2D} \widehat{\mathbf{p}}_{(j)}^2 \widehat{\mathbf{q}}_{(j)}^2 \right]$$

and is given by

$$\Sigma(\mathbf{k}) = \frac{\widehat{\mathbf{k}}_{(3)}^2}{2m} A_3(T) + \frac{\widehat{\mathbf{k}}_{(1)}^2}{2m} A_1(T) + \frac{\widehat{\mathbf{k}}_{(2)}^2}{2m} A_2(T). \quad (31)$$

The temperature dependent factors $A_j(T)$ are

$$\begin{aligned} A_1(T) &= \frac{a^2}{2D} \frac{|\lambda_1|^2}{|\lambda_3|^2} \frac{I_1^x}{I_3^x} v_0 \int_{\mathbf{q}} \langle n_{\mathbf{q}} \rangle_0 \widehat{\mathbf{q}}_{(1)}^2, \\ A_2(T) &= \frac{b^2}{2D} \frac{|\lambda_2|^2}{|\lambda_3|^2} \frac{I_2^x}{I_3^x} v_0 \int_{\mathbf{q}} \langle n_{\mathbf{q}} \rangle_0 \widehat{\mathbf{q}}_{(2)}^2, \\ A_3(T) &= \frac{2|\lambda_3|^2}{2D} v_0 \int_{\mathbf{q}} \langle n_{\mathbf{q}} \rangle_0 \widehat{\mathbf{q}}_{(3)}^2. \quad (32) \end{aligned}$$

They are dimensionless quantities that capture the effects of exciton-exciton interactions in two-level system by renormalizing exchange integrals $I_j^x \rightarrow I_j^x(T)$. Finally,

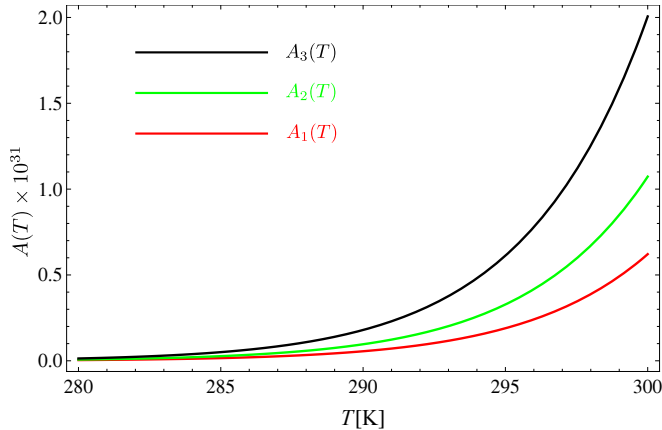


FIG. 7.
Renormalizing factors $A_j(T)$ defined in (32).

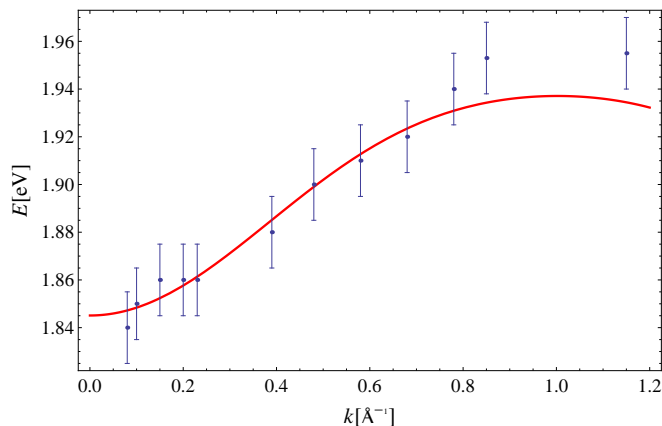


FIG. 8. Exciton dispersion along (100) direction. Experimental data are taken from [10]. Theoretical curve is obtained for: $\Delta = 1.90\text{eV}$ [33], $I_1^x = 5.7\text{meV}$, $I_2^x = 3.4\text{meV}$ and $I_3^x = 23.4\text{meV}$.

renormalized exciton energies read [18]

$$E_R(\mathbf{k}) = E(\mathbf{k}) - \Sigma(\mathbf{k}), \quad (33)$$

and the influence of exciton-exciton interactions at one-loop order can be seen from Fig. 7.

As noted in Introduction, the experimental data on exciton dispersion along (100) and (110) directions at lower temperatures are available [10]. One can see from Figs 8 and 9 that the effective model (18), with parameters $\Delta = 1.90\text{eV}$ [33], $I_1^x = 5.7\text{meV}$, $I_2^x = 3.4\text{meV}$ and $I_3^x = 23.4\text{meV}$ gives exciton dispersion in satisfying agreement with the experimental one. The only difference between two sets of parameters, describing experimental data obtained at 300K and 20K, is the value of the parameter Δ , which originates from the change of magnetic field \mathcal{H} in (2).

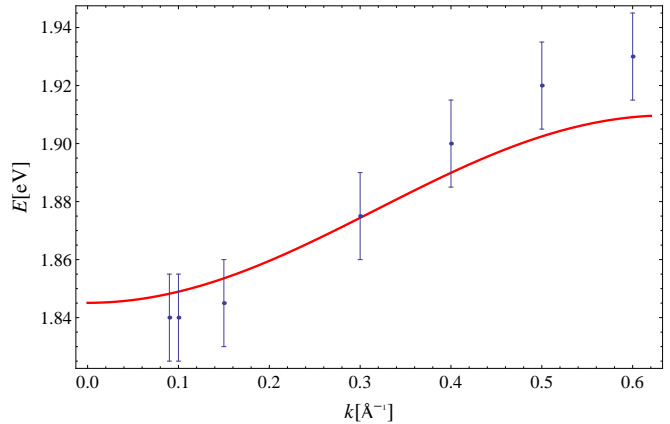


FIG. 9. Exciton dispersion along (110) direction. Experimental data are taken from [10]. Theoretical curve is obtained for: $\Delta = 1.90\text{eV}$ [33], $I_1^x = 5.7\text{meV}$, $I_2^x = 3.4\text{meV}$ and $I_3^x = 23.4\text{meV}$.

V. DISCUSSION

As seen from Fig. 7, the influence of exciton-exciton interactions is negligible at room temperatures. There are two main reasons for this. First, the exciton gap is huge – nearly two orders of magnitude larger than the greatest exchange integral. Second, excitons are derivatively coupled via interactions that are of the type occurring in the nonlinear σ models. Since these interactions include Laplacians, they tend to vanish at low energies. In fact, recent studies [39, 40] have shown that scattering amplitudes in a system governed by such interactions disappear as momenta of particles tend to zero. This interpretation is similar to the one given by Dyson in his analysis of ferromagnetic systems [41, 42]. On the other hand, as scattering amplitudes tend to zero regardless of exciton gap (i.e. fictitious external magnetic field of corresponding ferromagnetic system), it contradicts to the “hard sphere” picture of exciton dynamics from [20].

It is important to compare results from the present paper to the ones obtained by solving Bethe-Salpeter (BS) equations for many-body electron-hole system [13, 14]. First, the exciton dispersion obtained here is closer to experimental values. This is clearly seen by comparing Figures 2-5 from present paper to the results of Cudazzo et al. (see Figure 3 in [13]). Second, the exciton dispersion obtained with the help of the effective model in the present paper is much more robust against perturbative corrections. This may also be seen from Figs 3 and 4 from [13]: The dispersion obtained using flat HOMO-LUMO bands yields exciton dispersion close to 3.5eV, while those obtained using HOMO-LUMO with full dispersion are between 1.77eV and 1.8eV along (100) direction.

To conclude, we have analyzed the exciton dispersion in pentacene relying on the correspondence between Pauli (1) and Heisenberg (2) Hamiltonians. By fitting exchange integrals to the experimental data, we have obtained exciton dispersion that possesses the same periodicity as experimentally observed one. Also, our results provide an indirect confirmation that 2D model is in-

deed a minimal one that describes available experimental data on exciton dispersion. Further, we have shown that exciton-exciton interactions produce negligible effects to the one loop order. Because of that, we suggest that the influence of CT excitons in pentacene, which needs to be taken into account, may be less important than indicated in previous studies. It would be interesting to see experimental data on exciton dispersion along c^* axis and how this data would fit into existing models. Also, it is important to understand how to improve calculations based on BS equations to reach better agreement with experimental data on exciton dispersion and to test that approach for all four directions within Brillouin zone considered in

[3]. Therefore, further experimental and theoretical work is necessary before drawing final conclusion regarding the influence of CT excitons in pentacene.

ACKNOWLEDGMENTS

We are grateful to R. Schuster for sharing experimental data from [3] and for helpful discussions. We also wish to thank the referees for their helpful comments. This work was supported by the Serbian Ministry of Education and Science under Contract No. OI-171009 and by the Provincial Secretariat for High Education and Scientific Research of Vojvodina (Project No. APV 114-451-2201).

-
- [1] S. R. Forrest, *Nature* **428**, 911 (2004).
- [2] G. Li, V. Shrotriya, J. Huang, Y. Yao, T. Moriarty, K. Emery, and Y. Yang, *Nature Materials* **4**, 864 (2011).
- [3] R. Schuster, M. Knupfer, and H. Berger, *Phys. Rev. Lett.* **98**, 037402 (2007).
- [4] V. Agranovich and V. Ginzburg, *Crystal Optics with Spatial Dispersion and Excitons* (Springer, 1984).
- [5] V. Agranovich, *Excitations in organic solids* (Oxford University Press, 2008).
- [6] V. Rumyantsev, S. Fedorov, K. Gumennyk, M. Sychanova, and A. Kavokin, *Scientific reports* **4**, 6945 (2014).
- [7] V. Agranovich and G. Bassani, *Thin Films and Nanostructures (Electronic Excitations in Organic Based Nanostructures, Volume 31)* (New York: Elsevier Academic Press, 2003).
- [8] M. Schirter, S. Ivanov, J. Schulze, S. Polyutov, Y. Yan, T. Pullerits, and O. Khn, *Physics Reports* **567**, 1 (2015), excitonvibrational coupling in the dynamics and spectroscopy of Frenkel excitons in molecular aggregates.
- [9] B. Tošić, M. Pantić, and S. Lazarev, *Journal of Physics and Chemistry of Solids* **58**, 1995 (1997).
- [10] F. Roth, R. Schuster, A. Knig, M. Knupfer, and H. Berger, *The Journal of Chemical Physics* **136**, 204708 (2012).
- [11] F. Roth, B. Mahns, B. Büchner, and M. Knupfer, *Phys. Rev. B* **83**, 165436 (2011).
- [12] P. Cudazzo, M. Gatti, and A. Rubio, *Phys. Rev. B* **86**, 195307 (2012).
- [13] P. Cudazzo, M. Gatti, A. Rubio, and F. Sottile, *Phys. Rev. B* **88**, 195152 (2013).
- [14] P. Cudazzo, F. Sottile, A. Rubio, and M. Gatti, *Journal of Physics: Condensed Matter* **27**, 113204 (2015).
- [15] L. Kronik and J. B. Neaton, *Annual Review of Physical Chemistry* **67**, 587 (2016).
- [16] S. Sharifzadeh, P. Darancet, L. Kronik, and J. B. Neaton, *The Journal of Physical Chemistry Letters* **4**, 2197 (2013).
- [17] S. Weinberg, *The Quantum Theory of Fields II* (Cambridge University Press, 2010).
- [18] X. G. Wen, *Quantum Field Theory of Many Body Systems* (Oxford University Press, 2007).
- [19] T. Brauner, *Symmetry* **2**, 609 (2010).
- [20] V. Agranovich and B. Toshich, *Sov. Phys. JETP* **26**, 104 (1968).
- [21] S. V. Tyablikov, *Methods in the Quantum Theory of Magnetism* (Springer, 1967).
- [22] P. Frbrich and P. Kuntz, *Physics Reports* **432**, 223 (2006).
- [23] A. Auerbach, *Interacting electrons and quantum magnetism* (Springer, 2012).
- [24] E. Manousakis, *Rev. Mod. Phys.* **63**, 1 (1991).
- [25] W. Nolting and A. Ramakanth, *Quantum theory of magnetism* (Springer, 2009).
- [26] A. W. Sandvik and J. Kurkijärvi, *Phys. Rev. B* **43**, 5950 (1991).
- [27] M. R. Pantić, D. V. Kapor, S. M. Radošević, and P. M. Mali, *Solid State Communications* **182**, 55 (2014).
- [28] C. P. Hofmann, *Phys. Rev. B* **60**, 388 (1999).
- [29] C. P. Hofmann, *Phys. Rev. B* **86**, 054409 (2012).
- [30] J. Cornil, J. P. Calbert, and J. L. Brdas, *Journal of the American Chemical Society* **123**, 1250 (2001).
- [31] V. Stehr, J. Pfister, R. F. Fink, B. Engels, and C. Deibel, *Phys. Rev. B* **83**, 155208 (2011).
- [32] S. M. Radošević, M. S. Rutonjski, M. R. Pantić, M. V. Pavkov-Hrvojević, D. V. Kapor, and M. G. Škrinjar, *Solid State Communications* **151**, 1753 (2011).
- [33] M. Knupfer and H. Berger, *Chemical Physics* **325**, 92 (2006), electronic Processes in Organic Solids.
- [34] H. Marciniak, M. Fiebig, M. Huth, S. Schiefer, B. Nickel, F. Selmaier, and S. Lochbrunner, *Phys. Rev. Lett.* **99**, 176402 (2007).
- [35] S. M. Radošević, M. R. Pantić, M. V. Pavkov-Hrvojević, and D. V. Kapor, *Annals of Physics* **339**, 382 (2013).
- [36] S. M. Radošević, *Annals of Physics* **362**, 336 (2015).
- [37] H. Leutwyler, *Phys. Rev. D* **49**, 3033 (1994).
- [38] H. Watanabe and H. Murayama, *Phys. Rev. Lett.* **108**, 251602 (2012).
- [39] T. Brauner and M. F. Jakobsen, *Phys. Rev. D* **97**, 025021 (2018).
- [40] S. Gongyo, Y. Kikuchi, T. Hyodo, and T. Kunihiro, *Progress of Theoretical and Experimental Physics* **2016**, 083B01 (2016).
- [41] F. J. Dyson, *Phys. Rev.* **102**, 1217 (1956).
- [42] F. J. Dyson, *Phys. Rev.* **102**, 1230 (1956).